Ecotoxicology and Environmental Safety 280 (2024) 116533

Contents lists available at ScienceDirect

Ecotoxicology and Environmental Safety

journal homepage: www.elsevier.com/locate/ecoenv

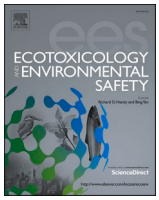

Heteroaggregation and deposition behaviors of carboxylated nanoplastics with different types of clay minerals in aquatic environments: Important role of calcium(II) ion-assisted bridging

Xiaoping Lin [a,b], Xin Nie [b,*], Ruiyin Xie [a,b], Zonghua Qin [b], Meimei Ran [b,c], Quan Wan [b,d], Jingxin Wang [a,*]

[a] Guangdong Provincial Engineering Research Center of Public Health Detection and Assessment, School of Public Health, Guangdong Pharmaceutical University, Guangzhou 510310, China
[b] State Key Laboratory of Ore Deposit Geochemistry, Research Center of Ecological Environment and Resource Utilization, Institute of Geochemistry, Chinese Academy of Sciences, Guiyang 550081, China
[c] School of Geographic and Environmental Sciences, Guizhou Normal University, Guiyang 550001, China
[d] CAS Center for Excellence in Comparative Planetology, Hefei 230026, China

ARTICLE INFO

Edited by: Professor Bing Yan

Keywords:
Clay minerals
Carboxylated polystyrene nanoplastics
Ca^{2+}-assisted bridging
Deposition
Electrostatic interactions

ABSTRACT

The widespread utilization of plastic products ineluctably leads to the ubiquity of nanoplastics (NPs), causing potential risks for aquatic environments. Interactions of NPs with mineral surfaces may affect NPs transport, fate and ecotoxicity. This study aims to investigate systematically the deposition and aggregation behaviors of carboxylated polystyrene nanoplastics (COOH-PSNPs) by four types of clay minerals (illite, kaolinite, Na-montmorillonite, and Ca-montmorillonite) under various solution chemistry conditions (pH, temperature, ionic strength and type). Results demonstrate that the deposition process was dominated by electrostatic interactions. Divalent cations (i.e., Ca^{2+}, Mg^{2+}, Cd^{2+}, or Pb^{2+}) were more efficient for screening surface negative charges and compressing the electrical double layer (EDL). Hence, there were significant increases in deposition rates of COOH-PSNPs with clay minerals in suspension containing divalent cations, whereas only slight increases in deposition rates of COOH-PSNPs were observed in monovalent cations (Na^{+}, K^{+}). Negligible deposition occurred in the presence of anions (F^{-}, Cl^{-}, NO^{3-}, CO_3^{2-}, SO_4^{2-}, or PO_4^{3-}). Divalent Ca^{2+} could incrementally facilitate the deposition of COOH-PSNPs through Ca^{2+}-assisted bridging with increasing $CaCl_2$ concentrations (0–100 mM). The weakened deposition of COOH-PSNPs with increasing pH (2.0–10.0) was primarily attributed to the reduce in positive charge density at the edges of clay minerals. In suspensions containing 2 mM $CaCl_2$, increased Na^{+} ionic strength (0–100 mM) and temperature (15–55 °C) also favored the deposition of COOH-PSNPs. The ability of COOH-PSNPs deposited by four types of clay minerals followed the sequence of kaolinite > Na-montmorillonite > Ca-montmorillonite > illite, which was related to their structural and surface charge properties. This study revealed the deposition behaviors and mechanisms between NPs and clay minerals under environmentally representative conditions, which provided novel insights into the transport and fate of NPs in natural aquatic environments.

1. Introduction

Plastic products are extensively used in daily life due to their light weight, corrosion resistance, stable chemical properties and low price. Approximately 12 billion tons of plastic waste will accumulate in the natural environment by 2050 due to the mismanagement (Chang et al., 2023; Geyer et al., 2017). These plastic wastes can be fragmented into smaller particles such as microplastics (MPs, 1 μm–5 mm) or further into nanoplastics (NPs, <1 μm) through the physical fragmentation, mechanical abrasion, chemical weathering, ultraviolet radiation, and the biological degradation, leading to the ubiquitousness of MPs and NPs in aquatic and soil environments (Vu et al., 2023; Yu et al., 2021; Zhang

* Corresponding authors.
E-mail addresses: xiaoping488@163.com (X. Lin), niexin2004@163.com (X. Nie), xry12128@163.com (R. Xie), qinzonghua@mail.gyig.ac.cn (Z. Qin), 3310264668@qq.com (M. Ran), wanquan@vip.gyig.ac.cn (Q. Wan), wjxdaxue@163.com (J. Wang).

https://doi.org/10.1016/j.ecoenv.2024.116533
Received 11 March 2024; Received in revised form 15 May 2024; Accepted 30 May 2024
Available online 7 June 2024

et al., 2023). Unlike bulk plastics, owing to their unique surface properties (i.e., high specific surface area and surface reactivity, abundant surface functional groups, as well as adsorption sites), NPs are prone to the adsorb and enrich the heavy metals, pathogenic microorganisms and organic contaminants, thereby affecting their migration, fate, bioavailability, reactivity and ecotoxicity in the ecosystem (Sun et al., 2021). The nanoscale size enables NPs to be easily ingested by the organisms and can even penetrate cell membranes, directly producing negative effects on specific cells, tissues, and organs (Ling et al., 2021). NPs could be accumulated by the marine and the freshwater organisms, ultimately affecting human health through the food chain (Yang et al., 2022). Nowadays, NPs have received considerable attention as an emerging contaminant for the hazardous effects on ecosystems (Ding et al., 2022; Zhang et al., 2023). Therefore, investigating the environmental behaviour of NPs is fundamental to evaluate their potential risks to human health.

Once discharged into aqueous environments, most NPs continue to undergo aging, transport, aggregation, and deposition, which inevitably affect their environmental fate and subsequent ecological risks. Aging processes, including the ultraviolet radiation, physical abrasion, chemical oxidation, and/or biodegradation, will alter the surface morphology and physicochemical properties of NPs (e.g., increasing surface roughness, oxygen-containing groups and negative surface charges), resulting in increased specific surface area, hydrophilicity, and adsorption ability for harmful contaminants (Li et al., 2022; Zhang et al., 2022). The transport and deposition behaviors of NPs in aquatic and soil environments can be affected by multiple factors, such as the physicochemical properties of NPs, the environmental factors, and the coexisting minerals. Previous studies have shown that natural minerals with large surface areas and functional groups were important components of sediments and soils, and had a high affinity for NPs (Lu et al., 2021). The interactions between NPs and minerals through electrostatic and/or hydrophobic interactions, ligand exchange-surface complexation, hydrogen bonding, van der Waals forces, bridging, and steric forces, have been found to be important mechanisms in governing the transport and deposition behaviors of NPs in aqueous environments as well as the ecotoxicity associated with various contaminants (Xia et al., 2021; Xie et al., 2023; Yang et al., 2022). Hence, understanding the deposition behaviors and corresponding mechanisms of aged NPs with minerals in natural aqueous environments is significant for assessing the ecological and human risks.

As a class of hydrated phyllosilicates, clay minerals are the most important and ubiquitous natural minerals in soils and aquifer sediments that inevitably interact with NPs and affect the environmental behaviors. Clay minerals are typically characterized by permanent and variable charge components. Variable charge components are susceptible to pH changes (Lu et al., 2021; Vu et al., 2023). The surface charge of 2:1 layer structure clay minerals (e.g., montmorillonite and illite) is dominated by permanent negative charges, whereas it is mainly governed by variable charges for 1:1 layer structure clay minerals (e.g., kaolinite) (Bergaya et al., 2006; Lu et al., 2021). Despite interactions (association) between plastic particles and minerals that have been reported, most of the previous studies have solely explored scenarios where heterogeneous aggregation occurs between large-sized MPs and a single clay mineral (Chang et al., 2023). Different types of clay minerals have different physicochemical properties, and may have markedly contrasting effects on the transport and deposition behaviors of NPs (Lu et al., 2016). Our previous research gained some fundamental understanding of the interaction mechanisms between NPs and clay minerals (Nie et al., 2023; Zeng et al., 2023). Notwithstanding, these chemical conditions do not represent the natural water composition, where the salinity (ionic strength of Na^{+}) or hardness (concentration of Ca^{2+} or Mg^{2+}) may have an interactive effect on the transport and deposition behaviors of NPs (Ling et al., 2021). Existing studies have shown that the transport of carboxylated NPs may be suppressed in subsurface environments because divalent cations can bind to the negatively charged sites on the clay mineral's surface through electrostatic attraction, promoting the retention of NPs on the surface (Torkzaban et al., 2012; Wang et al., 2020). To date, available data (or studies/publications) investigated related to the interactions between clay minerals and NPs under environmentally relevant concentrations of divalent electrolytes (e.g., Ca^{2+} or Mg^{2+}) remain scarce. In addition, ambient temperature varies with the season, the longitude and latitude, and the depth of the underground, but there are still limited researches on the temperature-dependent deposition of NPs (Singh et al., 2019). Thereupon, more detailed investigations are desired to understand fundamentally the effects of hydrochemical factors and clay mineral types on the deposition behaviors of aged NPs in environmentally relevant conditions.

Herein, carboxylated polystyrene nanoplastics (COOH-PSNPs) with a particle size of about 300 nm in diameter were employed as representative aged NPs, which have been widely used as surrogates of NPs in previous scientific studies (Nie et al., 2023; Yu et al., 2021). Illite, kaolinite and montmorillonite (Na-montmorillonite and Ca-montmorillonite), represented the most abundant clay minerals in soils and sediments (Ding et al., 2022; Wu et al., 2023), were thus selected as representative natural clay minerals. The impacts of various solution hydrochemical conditions (pH, temperature, ionic strength and type) on the deposition behavior of COOH-PSNPs by four types of clay minerals in the presence or absence of divalent background electrolytes ($CaCl_2$) were systematically examined to identify the prevailing factor and further elucidate the interaction mechanism between COOH-PSNPs and clay minerals.

2. Materials and methods

2.1. Nanoplastics and minerals

Carboxylated polystyrene nanoplastics (COOH-PSNPs, 2.5 % *w/v*, 5 mL) with an average diameter of 300 nm were procured from Shanghai Aladdin Biochemical Technology Co., Ltd. The commercial plastic suspensions were diluted to 125 mg/L with deionized water and used as a stock solution for subsequent experiments. Four types of clay minerals (illite, kaolinite, Na-montmorillonite, and Ca-montmorillonite) with micrometer sizes were purchased from Hunan Guzhang Shanlin Shiyu Mineral Co., Ltd. Other chemicals were of analytical reagent grade. All experimental solutions were prepared with ultrapure water.

2.2. Characterization

The morphology of the samples was characterized by scanning electron microscopy (SEM, Scios, FEI, US). The zeta potentials of clay minerals and COOH-PSNPs and the hydrodynamic diameters (D_h) of COOH-PSNPs were determined with a high-sensitivity zeta potential and particle size analyzer (Omni, Brookhaven Instruments, USA). All measurements were executed in triplicate and averaged. The attenuated total reflectance-Fourier transform infrared spectroscopy (ATR-FTIR, Vertex 70 spectrometer, BRUKER OPTICS, US) was employed to explore the changes in surface functional groups of the samples under different hydrochemical conditions in the wavelength range 4000–400 cm^{-1}, and the ATR-FTIR scan time of the samples was maintained at 32 scans. The characterization results of clay minerals and COOH-PSNPs are presented in Supplementary Information.

2.3. Deposition experiments of COOH-PSNPs with clay minerals

For a typical deposition experiment, 0.01 g of clay minerals and 100 mL of 20 mg/L COOH-PSNPs suspension were added to a 250 mL conical flask. The suspension concentration of COOH-PSNPs in prior studies was generally set at 20 mg/L (Li et al., 2022; Nie et al., 2023; Xie et al., 2023). The effects of pH, ionic strength, ionic type, temperature and $CaCl_2$ concentrations on the deposition of COOH-PSNPs with clay

minerals were studied by batch experiments. Various anions and cations exist universally in natural aquatic environments. In order to comprehensively understand the effects of ionic type on the deposition of COOH-PSNPs with clay minerals, various representative cations (NaCl, KCl, $CaCl_2$, $MgCl_2$, $CdCl_2$, or $PbCl_2$) or anions (NaCl, NaF, Na_2CO_3, $NaNO_3$, Na_2SO_4, or Na_3PO_4) were added into the solution. The widespread and substantial salinity and hardness in surface waters that might alter the deposition behavior of COOH-PSNPs onto clay minerals should not be negligible. The total hardness of water was dominated by Ca^{2+} and Mg^{2+}, with Ca^{2+} being significantly more abundant than Mg^{2+}, accounting for almost 70 %. The average total hardness of fresh water was approximately 2 mM (173–236.3 mg/L $CaCO_3$) (Roberts and Powell, 2003; Shariati-Rad and Heidari, 2021). The high deposition rate of COOH-PSNPs and clay minerals in the presence of Ca^{2+} was possibly attributed to bridging effects in which divalent cations serve as a bridge between the clay minerals and carboxyl functional groups on the COOH-PSNPs (Ling et al., 2021; Torkzaban et al., 2012). For this aim, the effect of $CaCl_2$ concentration (0–100 mM) on the deposition of COOH-PSNPs was investigated at initial pH 6.0 to confirm the role of divalent cations in the deposition process. A background Ca^{2+} concentration of 2 mM was selected to simulate natural waters for deposition experiments. The influence of ionic types at the same level was compared, and the concentration of various ions was also 2 mM, which was commonly employed in previous studies (Dong et al., 2021; Torkzaban et al., 2012). HCl and NaOH solutions were applied to adjust the initial suspension pH-value. To better simulate the natural aquatic environmental conditions, a near-neutral pH of 6.0 was selected for deposition experiments, except for the pH effect. The temperature of the reaction solution was maintained at 25 °C throughout the experiment period, except for the temperature effect. The mixtures were shaken in an orbital incubator shaker (ZWYR-D2403, Zhicheng, China) at 200 rpm. At various time intervals (0, 10, 30, 60, 120, 180, 300, 480 min), 10 mL of mixed suspension was sampled and centrifuged at 8000 rpm for 5 min, and then 5 mL supernatant was carefully taken out for subsequent analysis. Preliminary experiments showed that a reaction time of 8 hours was sufficient to achieve equilibrium. A similar experimental approach was applied to explore the influence of pH and temperature on COOH-PSNPs deposition, in which the experiments were performed at the initial solution pH-value range of 2.0–10.0 or at various temperatures (15, 25, 35, 45, and 55 °C). The concentration of COOH-PSNPs was determined at the maximum absorption wavelength (234 nm) using an ultraviolet-visible spectrophotometer (UV-Vis, Cary-300, Agilent, USA) (Nie et al., 2023; Xie et al., 2023; Zhang et al., 2023). The ratio of suspended concentration (C) to initial concentration (C_0) of COOH-PSNPs was used to calculate the deposition extent of COOH-PSNPs, and the normalized deposition curves were drawn by the relationship between C/C_0 and time (t). Each deposition experiment was repeated twice for obtaining the standard deviation. Thereafter, the solid samples were dried at 30 °C, and the morphology and surface functional groups were further observed by SEM and ATR-FTIR.

3. Results

3.1. Effect of ionic type

Fig. 1 shows the deposition curves of COOH-PSNPs with clay minerals in the presence of various cations or anions at initial pH 6.0. Mixing COOH-PSNPs with four types of the clay minerals showed that the concentrations of COOH-PSNPs in the solutions were stable. With the addition of NaCl, KCl, NaF, Na_2CO_3, $NaNO_3$, Na_2SO_4, or Na_3PO_4, negligible deposition of COOH-PSNPs by the clay minerals was also observed except for kaolinite. For kaolinite, adding 2 mM NaCl, KCl, and $NaNO_3$ led to approximately 28.2 %, 25.4 %, and 28.1 % of COOH-PSNPs deposited after 8 h, respectively. On the contrary, with the addition of $CaCl_2$, $MgCl_2$, $CdCl_2$, or $PbCl_2$, the concentrations of COOH-PSNPs remaining in the suspensions decreased significantly with time, suggesting divalent cations (Ca^{2+}, Mg^{2+}, Cd^{2+}, and Pb^{2+}) have significant enhancement effects on the deposition of COOH-PSNPs with clay minerals. The ability to enhance the deposition of COOH-PSNPs followed the sequence of $Pb^{2+} > Cd^{2+} \approx Mg^{2+} > Ca^{2+}$. For instance, in the presence of Ca^{2+}, approximately 23.9 %, 97.0 %, 58.8 %, and 46.5 % of COOH-PSNPs were deposited by illite, kaolinite, Na-montmorillonite, and Ca-montmorillonite after 8 h, respectively. By adding Pb^{2+}, COOH-PSNPs were deposited completely by illite, kaolinite, and Na-montmorillonite within 8 h, and approximately 85.2 % of COOH-PSNPs deposited by Ca-montmorillonite after 8 h. To further evaluate whether COOH-PSNPs deposited with clay minerals when COOH-PSNPs and clay minerals were copresent in suspensions containing various cations or anions, controlled experiments were conducted by mixing COOH-PSNPs with 2 mM cations or anions. We have also found (data not shown here) that the concentrations of COOH-PSNPs in solutions remained unchanged after 8 h.

3.2. Effect of $CaCl_2$ concentration

Fig. 2 shows that negligible deposition of COOH-PSNPs with clay minerals was observed at $CaCl_2$ concentrations of 0–0.1 mM, and the relative concentration (C/C_0) of COOH-PSNPs in the suspension after 8 h almost remained unchanged, except for kaolinite could deposit 38.7 % of COOH-PSNPs at 0.1 mM $CaCl_2$. Clearly, the deposition rates of COOH-PSNPs increased with $CaCl_2$ concentration from 2 to 100 mM, indicating that the extent of COOH-PSNPs deposition exhibits a high dependence on $CaCl_2$ concentration. For instance, in the presence of 2 mM $CaCl_2$, about 19.5 %, 98.1 %, 73.9 %, and 57.5 % of COOH-PSNPs were deposited with illite, kaolinite, Na-montmorillonite, and Ca-montmorillonite, respectively, after 8 h. When the $CaCl_2$ concentration reached 100 mM, almost all the COOH-PSNPs were removed from the suspension within just 1 h.

3.3. Effect of pH

The relative concentrations of COOH-PSNPs (C/C_0) remaining in the suspension as a function of deposition time and initial pH in the presence or absence of $CaCl_2$ indicated that pH had a significant effect on the deposition behavior of COOH-PSNPs. In the suspension without $CaCl_2$ (Fig. 3a, c, e, and g), when the initial pH-value increased from 2.0 to 10.0, the deposition rates of COOH-PSNPs declined from 70.5 %, 99.4 %, 79.7 %, and 83.0 % to nearly zero after 8 h of interaction with illite, kaolinite, Na-montmorillonite, and Ca-montmorillonite, respectively. COOH-PSNPs deposited only slightly with clay minerals in the pH range of 6.0–10.0, but began to be significantly deposited at acidic pH 2.0, indicating that the occurrence of deposition was highly dependent on pH. Interestingly, the deposition of COOH-PSNPs with clay minerals at pH ranging from 6.0 to 10.0 was remarkable for the suspensions containing 2 mM $CaCl_2$. Even when increasing the pH to 10.0 (Fig. 3b, d, f, and h), approximately 25.7 %, 84.7 %, 49.7 % and 45.0 % of COOH-PSNPs were deposited after mixing with illite, kaolinite, Na-montmorillonite, and Ca-montmorillonite for 8 h, respectively. Such a phenomenon again illustrates that Ca^{2+} plays a crucial role in controlling the deposition behavior of COOH-PSNPs. Based on the observations in Fig. 3, it was theoretically inferred that divalent cations and lower pHs could promote the deposition of COOH-PSNPs by increasing their affinity for clay minerals.

3.4. Effect of ionic strength

The effect of NaCl concentration (0–100 mM) on the deposition of COOH-PSNPs was examined at initial pH 6.0 and 2 mM $CaCl_2$ (Fig. 4). With the addition of 1 mM NaCl, the deposition curves of COOH-PSNPs almost overlapped with those of 0 mM NaCl. The deposition rates of COOH-PSNPs with clay minerals increased with increasing NaCl concentrations. As the NaCl concentration was 10 mM, deposition rates of

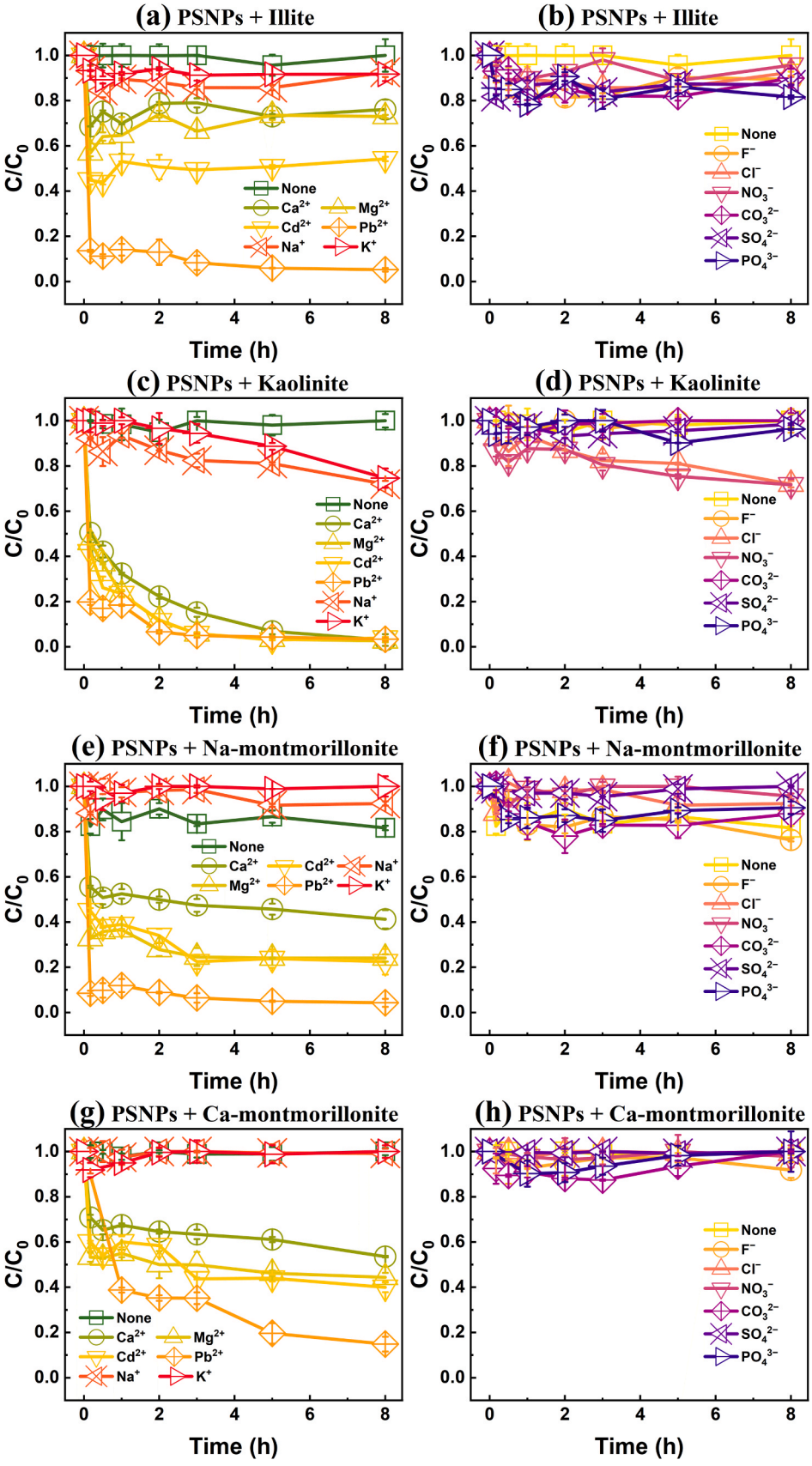

Fig. 1. Deposition curves of COOH-PSNPs with clay minerals in the presence of 2 mM various cations or anions at pH 6.0: (a, b) illite; (c, d) kaolinite; (e, f) Na-montmorillonite; (g, h) Ca-montmorillonite.

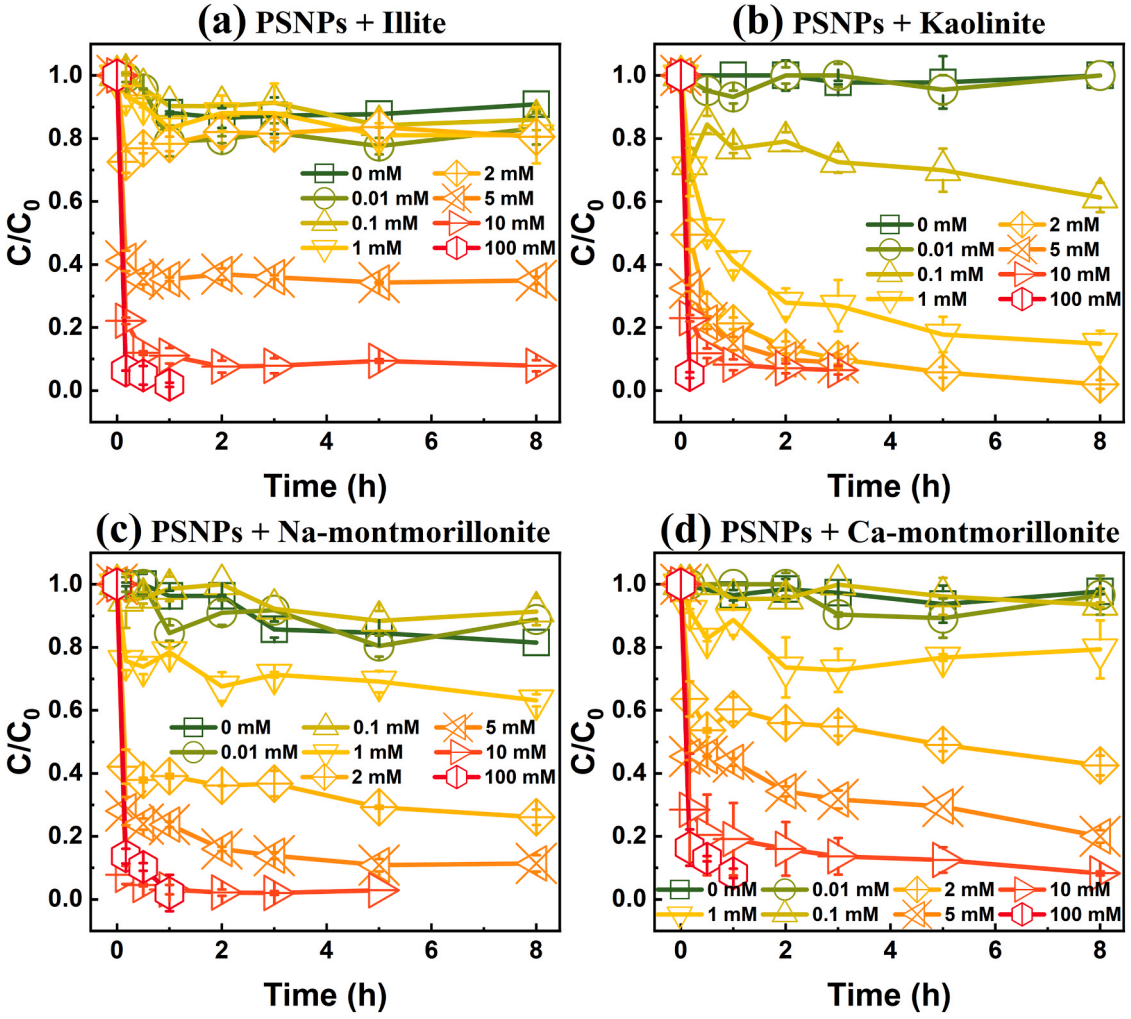

Fig. 2. Deposition curves of COOH-PSNPs with clay minerals at different $CaCl_2$ concentrations at pH 6.0: (a) Illite; (b) kaolinite; (c) Na-montmorillonite; (d) Ca-montmorillonite.

COOH-PSNPs with illite, kaolinite, Na-montmorillonite, and Ca-montmorillonite were approximately 34.8 %, 94.7 %, 57.7 %, and 46.4 %, respectively, after stirring for 8 h. At a concentration of 100 mM NaCl, approximately 57.1 %, 96.0 %, 73.2 %, and 73.0 % of COOH-PSNPs were deposited after 8 h in illite, kaolinite, Na-montmorillonite, and Ca-montmorillonite, respectively.

3.5. Effect of temperature

Fig. 5 presents the temperature-dependence experiments of COOH-PSNPs deposition performed at different temperatures with the initial pH 6.0 and 2 mM $CaCl_2$. With increasing temperatures from 15 to 55 °C, the deposition rates of COOH-PSNPs after 8 h of interaction with illite, kaolinite, Na-montmorillonite, and Ca-montmorillonite increased from 19.5 % to 54.8 %, 90.8–98.4 %, 40.0–89.0 %, and 39.5–80.5 %, respectively, indicating that higher temperatures facilitate the deposition.

4. Discussion

4.1. Influence of solution chemistry

4.1.1. Deposition mechanisms of cation-dependence

This study clearly demonstrated that electrostatic interactions dominated the interactions between COOH-PSNPs and clay mineral surfaces. The addition of 2 mM cations or anions alone could not cause the deposition of COOH-PSNPs. Therefore, the decrease in concentrations of COOH-PSNPs in solutions containing various cations or anions coexisting with clay minerals should undoubtedly be attributed to the deposition of COOH-PSNPs on clay minerals. In the suspensions without any cations or anions, the zeta potentials of illite, kaolinite, Na-montmorillonite, Ca-montmorillonite, and COOH-PSNPs were all negative at pH 6.0, leading to strong repulsive electrostatic forces and high energy barriers between highly negatively charged clay minerals and COOH-PSNPs, thus preventing the deposition of COOH-PSNPs (Fig. 6, Table S2). According to Derjaguin-Landau-Verwey-Overbeek (DLVO) theory, cations with the same valence should exhibit similar effects towards neutralizing surface negative charges (Li and Kobayashi, 2021). Monovalent cations (e.g., Na^+, K^+) compress EDL only to a certain extent. Divalent cations have a higher positive charge density to dramatically screen surface negative charges and compress EDL, leading to the electrostatic repulsive force and interaction energy barrier between clay minerals and COOH-PSNPs decreasing more than that of monovalent ions, as indicated by a significant decrease in their zeta potentials with increasing cation valence (Fig. 6a). Whereas anions will be repelled by negatively charged surfaces via electrostatic repulsion, which has a negligible effect on the surface charge of the negatively charged COOH-PSNPs and clay minerals (Fig. 6b). Therefore, divalent cations exhibited higher enhancement effects on the deposition extent of COOH-PSNPs than anions and monovalent cations. With the addition of

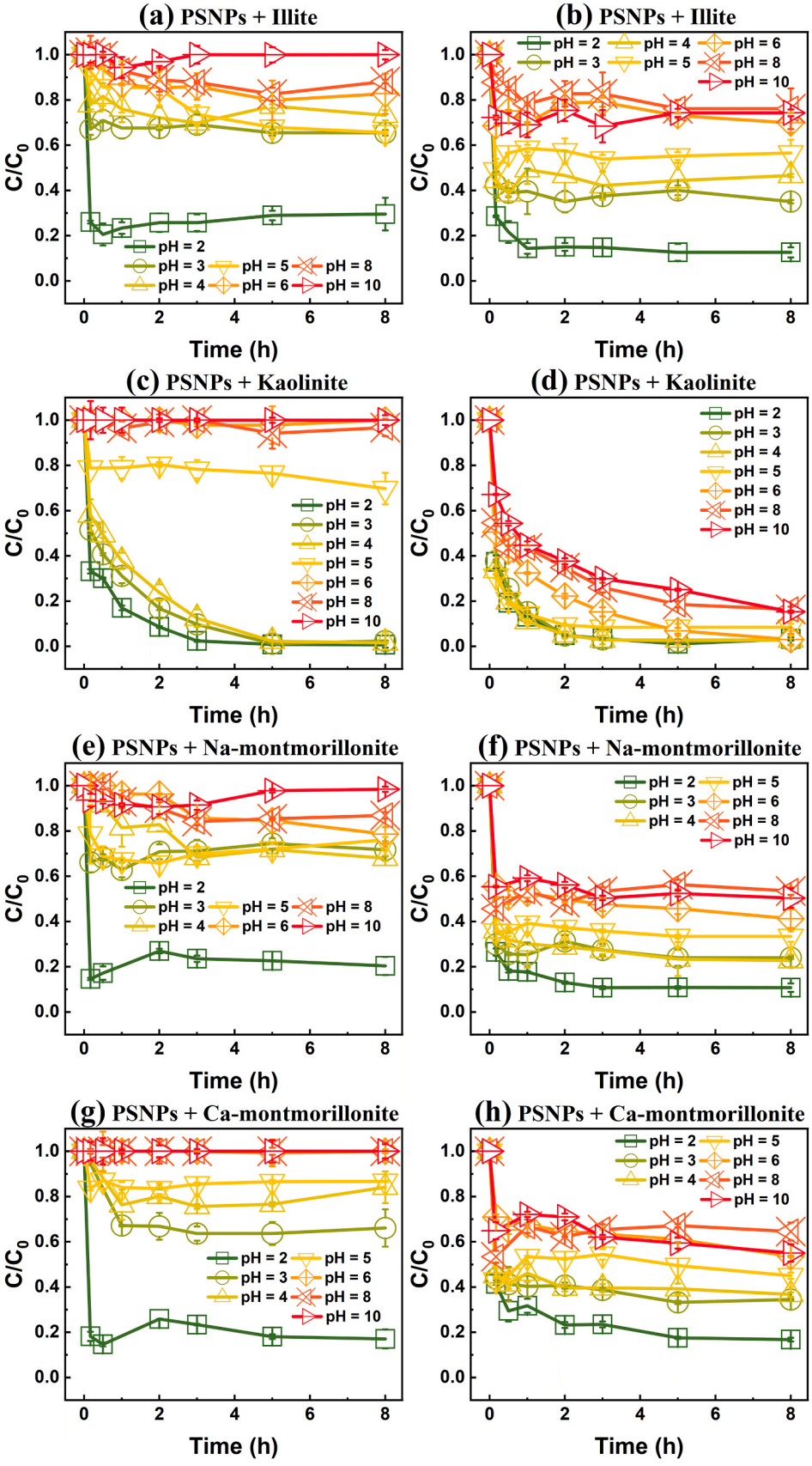

Fig. 3. Deposition curves of COOH-PSNPs with clay minerals at different pHs in the absence (a, c, e, and g) and presence (b, d, f, and h) of 2 mM $CaCl_2$: (a, b) illite; (c, d) kaolinite; (e, f) Na-montmorillonite; (g, h) Ca-montmorillonite.

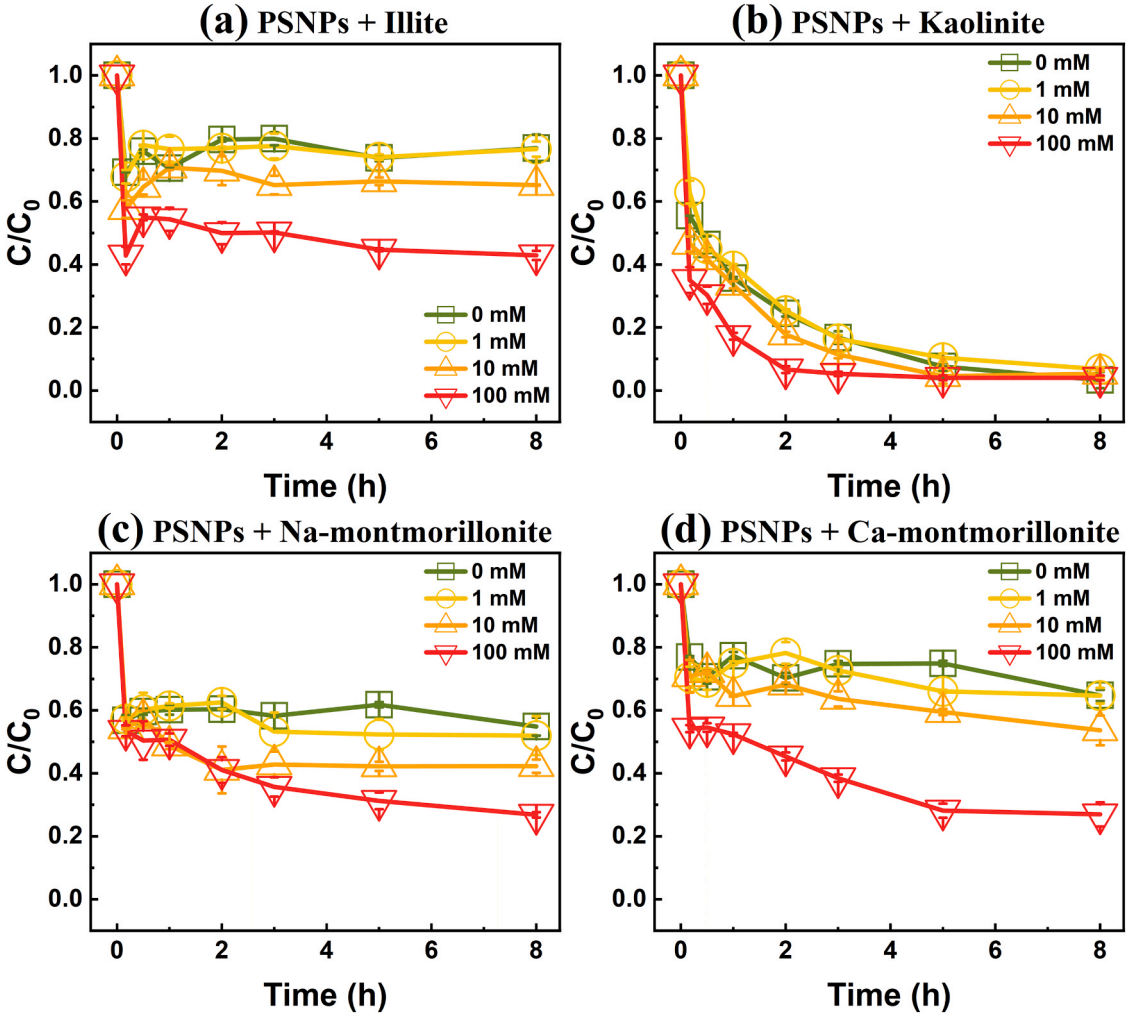

Fig. 4. Deposition curves of COOH-PSNPs with clay minerals at different ionic strengths in the presence of 2 mM $CaCl_2$ and at pH 6.0: (a) illite; (b) kaolinite; (c) Na-montmorillonite; (d) Ca-montmorillonite.

Cd^{2+}, Mg^{2+}, and Ca^{2+}, the zeta potentials of both COOH-PSNPs and clay minerals were maintained at similar values. More interestingly, in the presence of Pb^{2+}, the zeta potentials of illite, kaolinite, Na-montmorillonite, Ca-montmorillonite, and COOH-PSNPs at pH 6.0 were 31.6, 45.4, 23.2, 35.6, and 10.7 mV, respectively, suggesting that Pb^{2+} exhibits stronger capacities to penetrate the EDL to neutralize surface negative charges of both COOH-PSNPs and clay minerals more effectively, and even cause their potential reversal from negative to positive. Owing to its lower hydration layers, Pb^{2+} has a significantly stronger affinity for clay minerals and COOH-PSNPs than Cd^{2+}, Mg^{2+}, and Ca^{2+}. Cd^{2+}, Mg^{2+}, and Ca^{2+} were adsorbed onto clay mineral surfaces mainly via electrostatic interaction, outer-sphere surface complexation, or cation exchange reactions. Pb^{2+} could also be specifically adsorbed by clay minerals through surface complexation (inner--sphere complexes) or surface precipitation, and form strong covalent bonds to form stable complexes with COOH-PSNPs and both edge and planar sites on the clay mineral surface, which are more thermodynamically stable than non-specific interactions (Bergaya et al., 2006; Hizal and Apak, 2006). In the presence of the same cations except for Pb^{2+}, kaolinite showed the highest enhancement effect on COOH-PSNPs deposition, followed by montmorillonite and illite, suggesting that kaolinite has the greatest inhibitory effect on the mobility of COOH-PSNPs. SEM images of clay minerals mixed with COOH-PSNPs after 8 h in the presence of various cations at 2 mM are shown in Fig. S4. Only a few particles can be observed on the surface of various clay minerals with the addition of Na^+ and K^+. Clearly, numerous COOH-PSNPs particles attached to four clay mineral surfaces can be observed by adding various divalent cations, indicating the formation of COOH-PSNPs-clay mineral heteroaggregates, which was a predominant contributor to the increased deposition as well as decreased mobility of COOH-PSNPs.

Fig. S5 illustrates the variations of zeta potentials of COOH-PSNPs and clay minerals as a function of $CaCl_2$ concentration at pH 6.0. As shown, increasing $CaCl_2$ concentration from 0 to 0.01 mM led to the zeta potentials of COOH-PSNPs, illite, kaolinite, Na-montmorillonite and Ca-montmorillonite became less negative from −47.0 to −38.8, −40.7 to −29.3, −30.3 to −16.0, −35.7 to −25.8, and −27.0 to −17.7 mV, respectively. This may be attributed to an increase in ionic strength that screens the surface negative charges of COOH-PSNPs and clay minerals, implying that the electrostatic repulsion between them was weakened. The number of COOH-PSNPs on the clay minerals surface gradually increased with increasing $CaCl_2$ concentration.

Dynamic light scattering and homoaggregation experiments were also performed to exclude the effect of COOH-PSNPs homoaggregation on the deposition process. Figs. S1 and S2 showed that COOH-PSNPs exhibited little change in homoaggregation rates (<20 %) and D_h values (304.1 ± 5.3 nm) over a period of 8 h in the $CaCl_2$ concentrations ranging from 0 to 5 mM. When the concentration of $CaCl_2$ reached 10 mM, the D_h of COOH-PSNPs increased to ~330 nm after 8 h, and the homoaggregation rate of COOH-PSNPs reached 43.9 %. Almost all the

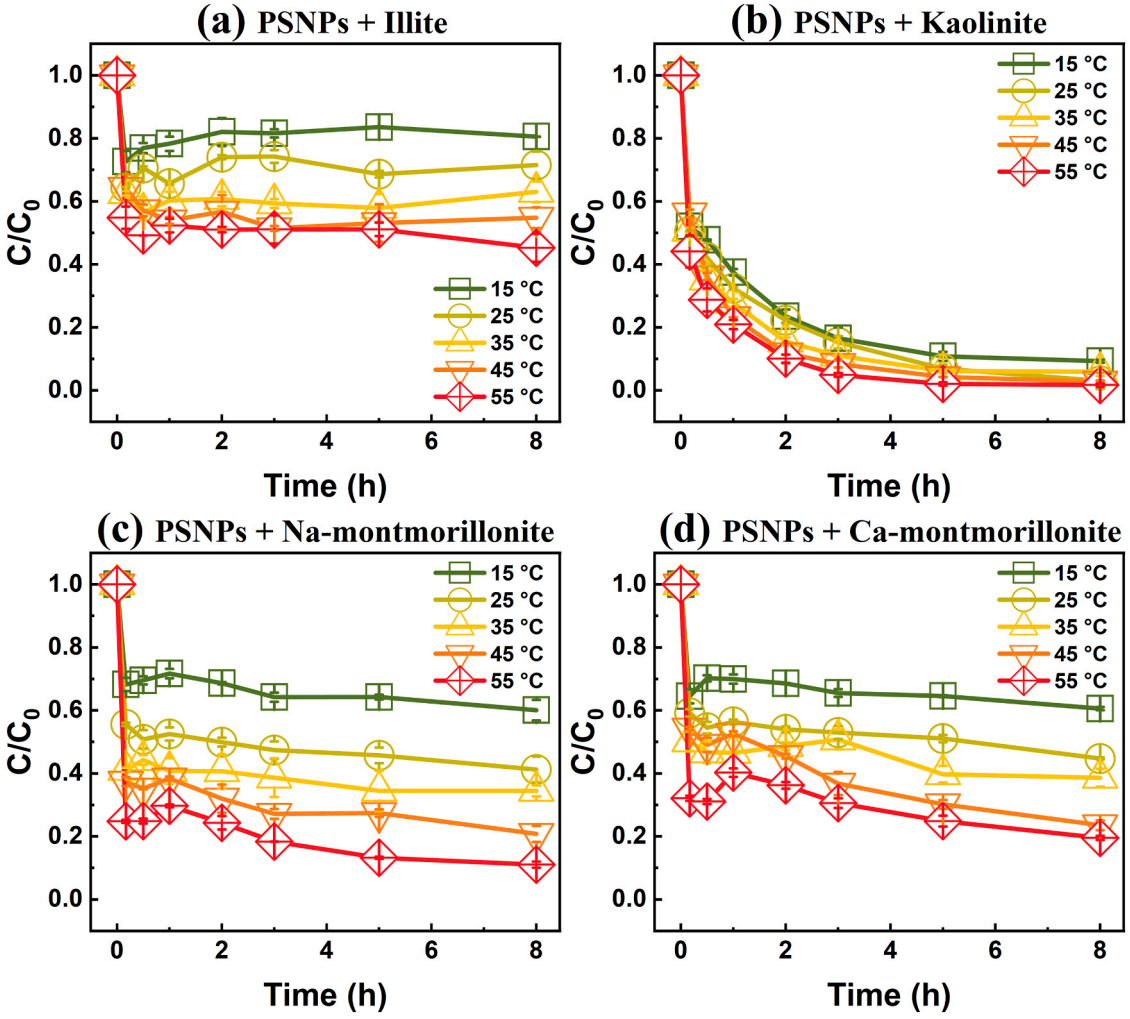

Fig. 5. Deposition curves of COOH-PSNPs with clay minerals at various temperatures in the presence of 2 mM $CaCl_2$ at pH 6.0: (a) illite; (b) kaolinite; (c) Na-montmorillonite; (d) Ca-montmorillonite.

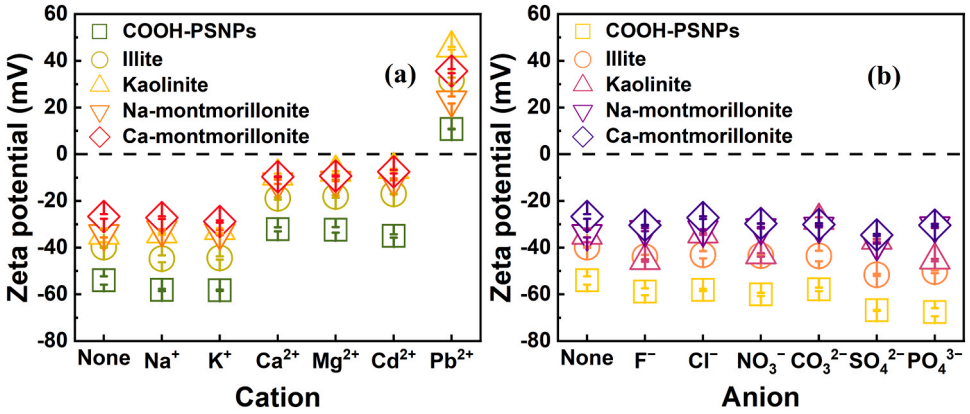

Fig. 6. Zeta potentials of clay minerals and COOH-PSNPs under the influence of 2 mM various ions at pH 6.0: (a) cations; (b) anions.

COOH-PSNPs aggregated at 100 mM $CaCl_2$ and rapidly formed large agglomerates (up to ~3000 nm). That was consistent with previous findings that high ionic strengths lead to a decrease in the stability of nanoparticle suspensions (Dong et al., 2019; Torkzaban et al., 2012). Such results implied that the deposition of COOH-PSNPs at ≤5 mM $CaCl_2$ should not be caused by homoaggregation, but by hetero-aggregation between COOH-PSNPs and clay minerals with the assistance of cation bridging.

The ATR-FTIR results of four clay minerals before and after the deposition experiments in the presence of different $CaCl_2$ concentrations are shown in Figs. 7a–d and S6. For COOH-PSNPs, the absorption peaks at 538, 699, 760, 1198 and 2923 cm^{-1} were attributed to C–H bending vibration, the peaks at 1452, 1492 and 1600 cm^{-1} were ascribed to aromatic structures, and the peak at 1730 cm^{-1} belonged to the

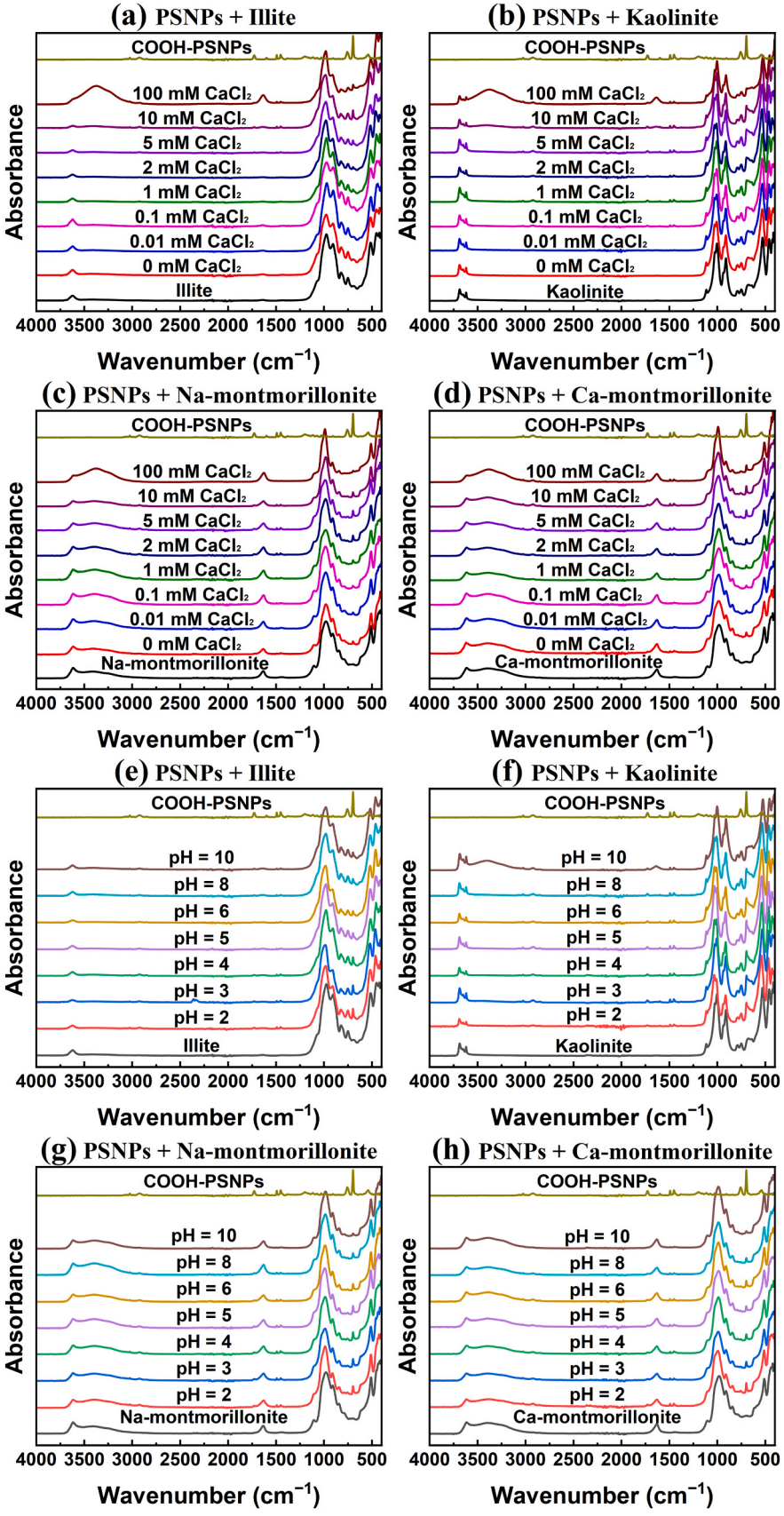

Fig. 7. Attenuated total reflectance-Fourier transform infrared spectra of clay minerals after 8 h of interaction with COOH-PSNPs under the influence of (a–d) different concentrations of $CaCl_2$ (pH 6.0) and (e–h) different pH: (a, e) illite; (b, f) kaolinite; (c, g) Na-montmorillonite; (d, h) Ca-montmorillonite.

O−C═O stretching vibration of the carboxyl groups (Xie et al., 2023). Clay minerals (illite, kaolinite, Na-montmorillonite, and Ca-montmorillonite) are mainly composed of Si−O−Si and Al−OH bonds, corresponding to absorption peaks around 1110–1114, 3620–3688, 906–974, 690–791, and 427–529 cm^{-1} (Vu et al., 2023). For illite, the absorption peaks at 1627 and 3620 cm^{-1} were assigned to the O−H stretching vibration and H−O−H bending vibration, respectively. For kaolinite, the peaks at 3619, 3652 and 3688 cm^{-1} were ascribed to the vibration of O−H, while 1629 and 3374 cm^{-1} were the vibration peaks of adsorbed water (H−O−H). For Na-montmorillonite and Ca-montmorillonite, the peak at 3620 cm^{-1} was ascribed to the stretching vibration of the silanol group (Si−OH), whereas the peaks around 1630 cm^{-1} and the board adsorption peak at 3380 cm^{-1} were attributed to the vibration of interlayer water molecules in the silicate matrix and surface adsorbed water, respectively (Maged et al., 2020; Vu et al., 2023; Zhang et al., 2022). The peak intensity of adsorbed water for illite, kaolinite, Na-montmorillonite, and Ca-montmorillonite around 3382 and 1629 cm^{-1} gradually enhanced with increasing $CaCl_2$ concentration. Simultaneously, their Si−O and Si−O−Si peaks near 908 cm^{-1} gradually weaken (Fig. S6). Cation could be adsorbed onto clay minerals by cation exchange or by the formation of inner- or outer-sphere complexes through Si−O and Al−O groups, etc. Specifically, the strong hydration of Ca^{2+} and water molecules attenuated the stretching vibrations of Si−O and Si−O−Si, indicating significant Ca^{2+} adsorption on the surface of clay minerals that is positively correlated with $CaCl_2$ concentration (Bergaya et al., 2006; Brião et al., 2021). As mentioned above, the deposition behavior of clay minerals and COOH-PSNPs in the presence of Pb^{2+} differs from that of Ca^{2+}. Thus, a parallel comparison with Pb^{2+} validates that the peaks of adsorbed water on the mineral surface can be used as evidence for the interaction of Ca^{2+} with clay minerals (Figs. S7 and S8). All the positions of clay minerals adsorption peaks did not shift significantly after interaction with COOH-PSNPs (Fig. 7a–d). The characteristic absorption peaks of COOH-PSNPs were apparently observed at $CaCl_2$ concentrations of 5, 0.1, 1, and 1 mM for illite, kaolinite, Na-montmorillonite, and Ca-montmorillonite, respectively, which verified the aforementioned results (Fig. 2). The intensities of characteristic peaks associated with COOH-PSNPs gradually increased with $CaCl_2$ concentration, whereas the peak intensity of H−O−H decreased, indicating that more COOH-PSNPs were adsorbed by clay minerals at higher concentrations of $CaCl_2$. Ca^{2+} with a small hydration radius is sufficient for the formation of an inner-sphere complex with COOH-PSNPs, which can provide abundant binding sites due to the abundance of carboxyl groups (Xia et al., 2021). Hence, the deposition of COOH-PSNPs with clay minerals may occur through cation bridging. Fig. S9 shows the SEM images of four clay minerals before and after being mingled with COOH-PSNPs at different $CaCl_2$ concentrations, where the attachment of COOH-PSNPs to the clay mineral surface is visible. Also, COOH-PSNPs remain heteroagglomerated in a relatively monodisperse form at lower $CaCl_2$ concentrations, whereas homoaggregation occurs at higher $CaCl_2$ concentrations. This indicates that negligibly the deposition behavior of COOH-PSNPs affected by homoaggregation at lower $CaCl_2$ concentrations.

As noted in previous studies, interlayer cation exchange and protonation or deprotonation of hydroxyl groups at the edge surfaces of clay minerals can alter the pH of the suspension (Zeng et al., 2023). It changes in the final pH during the deposition experiments in the absence and presence of $CaCl_2$ were further compared, and the results are shown in Table S1 and Fig. S3. The initial pH of COOH-PSNPs suspensions was 6.0. After mixing with illite, kaolinite, Na-montmorillonite and Ca-montmorillonite, the final pH rose to 6.42, 6.84, 7.51 and 6.89 after 8 h, respectively. Intriguingly, the change in the final pH for the mixture suspensions containing 2 mM $CaCl_2$ was not pronounced, especially for that of Na-montmorillonite and Ca-montmorillonite. This may also be related to their water absorption mechanisms mediated by Ca^{2+}.

Under the same conditions, the highest rates of COOH-PSNPs deposited were observed on kaolinite, followed by Na-montmorillonite, Ca-montmorillonite, illite. By combining all the results, the deposition mechanism of divalent cations dominated by cation-bridging is again confirmed. In addition, the spillover of the electric double layer of negatively charged basal plane surfaces (C_f) may screen the coulombic attraction of the edges (C_e) to COOH-PSNPs at low $CaCl_2$ concentrations, whereas the C_f spillover effect will be weakened at higher $CaCl_2$ concentrations, and thus heteroaggregation between COOH-PSNPs and clay minerals may occur (Singh et al., 2019; Ye et al., 2022).

In general, the absolute zeta potentials showed downward trends with increasing ionic strength (Fei et al., 2022). However, the zeta potentials of illite, kaolinite, Na-montmorillonite, Ca-montmorillonite, and COOH-PSNPs became from −18.5 to −33.1, −8.1 to −23.1, −11.1 to −31.4, −8.4 to −28.9, and −31.7 to −40.3 mV, respectively, with the addition of NaCl from 0 to 100 mM in the presence of 2 mM $CaCl_2$ (Fig. S10). This phenomenon could be accounted for by the enhanced competitive effects of coexisting cations on the finite adsorption sites, as well as the exchange of adsorbed Ca^{2+} with high-concentration cations (Gao et al., 2021). In the coexistence of $CaCl_2$ and NaCl, the surface adsorption of Ca^{2+} was significantly higher than that of Na^+ when their concentrations were not much different (Bergaya et al., 2006; Torkzaban et al., 2012). The variation in zeta potentials was found to be minimal for NaCl concentrations of 0–10 mM, thus the deposition behavior was driven mainly by Ca^{2+} bridging. At NaCl concentrations up to 100 mM, the elevated ionic strength compressed the EDL and lowered the repulsive energy barriers between interacting clay minerals and COOH-PSNPs, resulting in the dominance of van der Waals interaction (Ling et al., 2022; Wang et al., 2020). The Ca^{2+} adsorbed on the surface and interlayer, meanwhile, was gradually replaced by Na^+ through the cation exchange reaction. Nevertheless, the actual exchange of Na^+ with Ca^{2+} is less than 2:1, resulting in decreased positive charges on their surfaces. This explains why more negative zeta potentials were observed with the addition of NaCl in the present study. Furthermore, since the total Ca^{2+} concentration in the system is constant, thus implying an increase in free Ca^{2+} concentration in solution, the bridging effect may be primarily implemented through this fraction of Ca^{2+} outside the Stern layer of EDL. The more Ca^{2+} is replaced by Na^+ inside the Stern layer of EDL, the more significant the bridging effect and the faster the deposition rates. Also, COOH-PSNPs are more likely to form homoaggregates under high ionic strength (Fei et al., 2022). Therefore, the deposition rates of COOH-PSNPs increased with NaCl concentration due to the combination effect of Ca^{2+} bridging, van der Waals attraction, and EDL compression.

4.1.2. Deposition mechanisms of pH-dependence

The influence of pH on the surface charges of clay minerals and COOH-PSNPs was significant. As pH increased from 2.0 to 12.0, the zeta potentials of illite, kaolinite, Na-montmorillonite, Ca-montmorillonite and COOH-PSNPs became more negative from −32.8 to −47.9, 7.2 to −48.8, −36.3 to −35.3, −27.7 to −31.8 and −40.8 to −74.2 mV, respectively (Fig. S11a). For both COOH-PSNPs and clay minerals, the negative zeta potentials increase with pH, which was attributed to their surface deprotonation as well as the increase of negative surface charges, leading to more negative zeta potentials under alkaline conditions (Ling et al., 2021), which increased the energy barriers and electrostatic repulsion between particles and enhanced their stability, preventing the occurrence of aggregation and deposition. Whereas the addition of 2 mM $CaCl_2$ significantly reduces their zeta potentials over the pH range we observed (Fig. S11b). The ATR-FTIR spectra of clay minerals and COOH-PSNPs before and after deposition under different pHs are illustrated in Figs. 7e–h and S12–14. Regardless of $CaCl_2$ presence or not, the adsorption peaks in four clay minerals under different pHs remained nearly unchanged (Figs. S12, S13). In the absence of $CaCl_2$, COOH-PSNPs-associated characteristic peaks (699, 1452, 1492, and 1730 cm^{-1}) could only be observed at pH below 2.0, 4.0, 5.0, and

5.0 on illite, kaolinite, Na-montmorillonite, and Ca-montmorillonite, respectively (Fig. S14). In the presence of $CaCl_2$, the characteristic absorption peaks of COOH-PSNPs were obviously observed on illite, kaolinite, Na-montmorillonite and Ca-montmorillonite at pH 10.0, and the peak intensities increased gradually with decreasing pH (Fig. 7e–h). Clearly, the coexistence of Ca^{2+} promotes the deposition of COOH-PSNPs with clay minerals.

4.1.3. Deposition mechanisms of COOH-PSNPs with different types of clay mineral

Clay minerals have various isomorphic substitutions, which create permanent negative charged C_f (pH-independent charges) on the silica basal planes and variable charged C_e (pH-dependent charges) on the edge surfaces. The charge type and density controlled by the protonation and deprotonation of the amphoteric Si–OH and Al–OH groups at the edges of different clay minerals are also different (Wu et al., 2023; Ye et al., 2022). An excess of protons produces positive edge charges when the pH is below the point of zero edge charge ($pH_{PZC\text{-}edge}$), and the density of positive charges increases with decreasing pH ($Al{-}OH + H^+ \Leftrightarrow Al{-}OH_2^+$). Therefore, heteroaggregation between negatively charged COOH-PSNPs and positively charged edges of clay minerals may occur at low pH. Negative charges are created by the dissociation of silanol and aluminol groups ($Al{-}OH + OH^- \Leftrightarrow AlO^-$, $Si{-}OH + OH^- \Leftrightarrow Si{-}O^-$). The $pH_{PZC\text{-}edge}$ of aluminum and silanol groups at the edges of kaolinite, montmorillonite and illite is close to 6.0–6.5, 6.5, and 2.5, respectively, and thus both positively charged C_e and permanently negatively charged C_f are present on kaolinite and montmorillonite surfaces at pH 6.0, while both C_f and C_e are negatively charged for illite at the same condition (Lu et al., 2021, 2016). However, negligible deposition of COOH-PSNPs with all clay minerals was observed without the addition of any cations. This is because the negative EDL extending from the C_f can spill over into the edge region and screen C_e columbic attraction for COOH-PSNPs (Nie et al., 2023), as validated by their zeta potentials, which indicated that the net charge of all clay minerals was negative at pH 6.0. The surface potentials of 2:1 clay minerals are dominated by the pH-insensitive C_f (Lu et al., 2021). For two 2:1 clay minerals, the zeta potentials of montmorillonite slightly varied with pH compared to illite, indicating that pH has less influence on the zeta potentials of montmorillonite than illite (Fig. S11a) (Wu et al., 2023). Despite this, the surface potentials of illite were still more negative than those of montmorillonite at the same pH (e.g., −39.8, −33.9, and −26.6 mV for illite, Na-montmorillonite and Ca-montmorillonite at pH 6.0, respectively), which led to a greater inhibition of COOH-PSNPs deposition with illite. For both types of montmorillonite, similar COOH-PSNPs depositions were observed. Kaolinite is a 1:1 clay mineral with more C_e and fewer C_f in comparison with montmorillonite and illite owing to its limited isomorphic substitutions and higher aspect ratio (thickness/diameter ratio) of the particles, resulting in a reduced C_f spillover effect for screening the positive edge charges (Bergaya et al., 2006; Lu et al., 2016). The zeta potentials of kaolinite were found to vary significantly with pH, become less negative with decreasing pH, and even turn positive at pH 2.0 (7.2 mV). This is attributed to the edge area of kaolinite occupies a significantly higher total surface area than that of montmorillonite and illite. The overall net charges of kaolinite significantly became less negative by adding divalent cations (Borst et al., 2020). Thus, compared to montmorillonite and illite, kaolinite possesses more positively charged edge sites on its surface, which will be more conducive to the deposition of negatively charged COOH-PSNPs (Ye et al., 2022).

4.1.4. Deposition mechanisms of temperature-dependence

The zeta potentials of both COOH-PSNPs and clay minerals were also dependent on temperature. Specifically, when the temperature was increased from 15 to 55 °C, the zeta potentials of illite, kaolinite, Na-montmorillonite, Ca-montmorillonite and COOH-PSNPs changed from −20.4 to −8.5, −9.3 to −4.1, −15.0 to −5.3, −10.8 to −5.0, and −38.6 to −17.1 mV, respectively, and became less negative at higher temperatures (Fig. S15). This implies that increasing temperature weakens the EDL repulsion between COOH-PSNPs and clay minerals, and the deposition process should be endothermic (Ling et al., 2022). The less negative zeta potentials can be attributed to the reduced dissociation extent of −OH/−COOH and the number of negative charges on the surfaces of COOH-PSNPs and clay minerals (Zeng et al., 2023). Higher temperatures could enhance the Brownian motion, kinetic energy, and chemical attachment of particles, which is beneficial for improving the collision frequency and heteroaggregation between COOH-PSNPs and clay minerals (Ling et al., 2021, 2022). Besides, increasing temperature facilitates the penetration of small-hydration-radius cations (i.e., Ca^{2+}) into the interlayer of clay minerals and adsorption on the surface (Bergaya et al., 2006). And it also promoted the dissolution of clay minerals, increased the ionic strength of the suspension, and reduced the negative zeta potentials of both COOH-PSNPs and clay minerals, thereby reducing their electrostatic repulsion (Cama et al., 2002; Zeng et al., 2023). As such, increases in temperatures lead to higher deposition rates.

4.2. Environmental implications

Nanoplastics have been increasingly identified in aquatic ecosystems in recent decades. Since nanoplastics can adsorb and transport metallic and organic contaminants, their accumulation in aquatic environments increases the risk of hazardous substances' transmission through the food chain to humans (Sun et al., 2021). Much of the current research related to nanoplastics has focused on the environmental behaviors of pristine nanoplastics, while the behavior of aged nanoplastics neglected. Aging processes alter nanoplastics physicochemical properties, thereby significantly increasing their ability to adsorb environmental contaminants. However, divalent cations (e.g., Ca^{2+}) may bridge oxygen-containing functional groups of nanoplastics to soil and sediment surfaces, leading to their high deposition and mobile limitation (Wang et al., 2020). In freshwater, estuaries, and marines, where various clay minerals are ubiquitous and divalent cation concentrations are within the corresponding ranges, aged nanoplastics are likely to be deposited by clay minerals due to divalent cation-assisted bridging. Herein, the effects of four clay minerals (illite, kaolinite, Na-montmorillonite, and Ca-montmorillonite) ubiquitous in soil and aquifer sediments on the deposition of aged nanoplastics (COOH-PSNPs) under ambient environmental conditions (pH, temperature, ionic strength and type) were systematically investigated. Our findings provide theoretical and technical foundations for the prediction, prevention, and control of nanoplastics contamination in natural waters, with significant references and underlying applications for public health.

5. Conclusions

Our results indicated that divalent cations contributed more effectively to the deposition of COOH-PSNPs with clay minerals due to the additional cation-bridging effect, higher EDL compression, and charge neutralization. With decreasing pH, the deposition of COOH-PSNPs increased both in the presence and absence of Ca^{2+}. Increasing Ca^{2+} concentration, Na^+ ionic strength, and temperature could suppress the EDL repulsion between particles and thus facilitate the deposition of COOH-PSNPs with clay minerals. The deposition rate of COOH-PSNPs mediated by Ca^{2+} showed a trend of kaolinite > Na-montmorillonite ≈ Ca-montmorillonite > illite, and the deposition of COOH-PSNPs was clearly controlled by the structural and surface charge properties of the four clay minerals. Overall, the interaction between COOH-PSNPs and clay minerals in natural aqueous environments is mainly mediated through the bridging effects of divalent cations. Outcomes of this study will help to comprehensively understand the transport and deposition mechanisms of NPs in natural environments, and can also provide new insights for assessing the environmental behaviors of NPs on Earth's surface.

CRediT authorship contribution statement

Xiaoping Lin: Writing – original draft, Methodology, Data curation. Xin Nie: Writing – review & editing, Writing – original draft, Visualization, Project administration, Methodology, Investigation, Funding acquisition, Formal analysis, Data curation, Conceptualization. **Ruiyin Xie:** Methodology, Data curation. **Zonghua Qin:** Methodology, Formal analysis. **Meimei Ran:** Data curation. **Quan Wan:** Supervision, Project administration, Conceptualization. **Jingxin Wang:** Writing – review & editing, Writing – original draft, Methodology, Conceptualization.

Declaration of Competing Interest

The authors declare that they have no known competing financial interests or personal relationships that could have appeared to influence the work reported in this paper.

Data availability

Data will be made available on request.

Acknowledgments

This work was financially supported by the A-type Strategic Priority Program of the Chinese Academy of Sciences (No. XDA0430103), National Natural Science Foundation of China (Nos. 41902041 and 41872046), Guizhou Provincial Science and Technology Projects (No. [2020]1Z039).

Appendix A. Supporting information

Supplementary data associated with this article can be found in the online version at doi:10.1016/j.ecoenv.2024.116533.

References

Bergaya, F., Theng, B.K.G., Lagaly, G., 2006. Handbook of Clay Science. Vol 1 Developments in Clay Science. Elsevier.

Borst, A.M., Smith, M.P., Finch, A.A., Estrade, G., Villanova-de-Benavent, C., Nason, P., et al., 2020. Adsorption of rare earth elements in regolith-hosted clay deposits. Nat. Commun. 11 https://doi.org/10.1038/s41467-020-17801-5.

Brião, Gd.V., da Silva, M.G.C., Vieira, M.G.A., 2021. Efficient and selective adsorption of neodymium on expanded vermiculite. Ind. Eng. Chem. Res. 60, 4962–4974. https://doi.org/10.1021/acs.iecr.0c05979.

Cama, J., Metz, V., Ganor, J., 2002. The effect of pH and temperature on kaolinite dissolution rate under acidic conditions. Geochim. Et. Cosmochim. Acta 66, 3913–3926. https://doi.org/10.1016/s0016-7037(02)00966-3.

Chang, B., He, B., Cao, G., Zhou, Z., Liu, X., Yang, Y., et al., 2023. Co-transport of polystyrene microplastics and kaolinite colloids in goethite-coated quartz sand: Joint effects of heteropolymerization and surface charge modification. Sci. Total Environ. 884 https://doi.org/10.1016/j.scitotenv.2023.163832.

Ding, L., Yu, X., Guo, X., Zhang, Y., Ouyang, Z., Liu, P., et al., 2022. The photodegradation processes and mechanisms of polyvinyl chloride and polyethylene terephthalate microplastic in aquatic environments: important role of clay minerals. Water Res. 208 https://doi.org/10.1016/j.watres.2021.117879.

Dong, S., Cai, W., Xia, J., Sheng, L., Wang, W., Liu, H., 2021. Aggregation kinetics of fragmental PET nanoplastics in aqueous environment: complex roles of electrolytes, pH and humic acid. Environ. Pollut. 268 https://doi.org/10.1016/j.envpol.2020.115828.

Dong, Z., Zhang, W., Qiu, Y., Yang, Z., Wang, J., Zhang, Y., 2019. Cotransport of nanoplastics (NPs) with fullerene (C_{60}) in saturated sand: effect of NPs/C_{60} ratio and seawater salinity. Water Res. 148, 469–478. https://doi.org/10.1016/j.watres.2018.10.071.

Fei, J., Xie, H., Zhao, Y., Zhou, X., Sun, H., Wang, N., et al., 2022. Transport of degradable/nondegradable and aged microplastics in porous media: effects of physicochemical factors. Sci. Total Environ. 851 https://doi.org/10.1016/j.scitotenv.2022.158099.

Gao, X., Hassan, I., Peng, Y., Huo, S., Ling, L., 2021. Behaviors and influencing factors of the heavy metals adsorption onto microplastics: a review. J. Clean. Prod. 319 https://doi.org/10.1016/j.jclepro.2021.128777.

Geyer, R., Jambeck, J.R., Law, K.L., 2017. Production, use, and fate of all plastics ever made. Sci. Adv. 3, e1700782 https://doi.org/10.1126/sciadv.1700782.

Hizal, J., Apak, R., 2006. Modeling of copper(II) and lead(II) adsorption on kaolinite-based clay minerals individually and in the presence of humic acid. J. Colloid Interface Sci. 295, 1–13. https://doi.org/10.1016/j.jcis.2005.08.005.

Li, Q., Bai, Q., Sheng, X., Li, P., Zheng, R., Yu, S., et al., 2022. Influence of particle characteristics, heating temperature and time on the pyrolysis product distributions of polystyrene micro- and nano-plastics. J. Chromatogr. A 1682. https://doi.org/10.1016/j.chroma.2022.463503.

Li, M., Kobayashi, M., 2021. The aggregation and charging of natural clay allophane: critical coagulation ionic strength in the presence of multivalent counter-ions. Colloids Surf. A: Physicochem. Eng. Asp. 626 https://doi.org/10.1016/j.colsurfa.2021.127021.

Ling, X., Yan, Z., Lu, G., 2022. Vertical transport and retention behavior of polystyrene nanoplastics in simulated hyporheic zone. Water Res. 219 https://doi.org/10.1016/j.watres.2022.118609.

Ling, X., Yan, Z., Liu, Y., Lu, G., 2021. Transport of nanoparticles in porous media and its effects on the co-existing pollutants. Environ. Pollut. 283 https://doi.org/10.1016/j.envpol.2021.117098.

Lu, T., Gilfedder, B.S., Peng, H., Niu, G., Frei, S., 2021. Effects of clay minerals on the transport of nanoplastics through water-saturated porous media. Sci. Total Environ. 796, 148982 https://doi.org/10.1016/j.scitotenv.2021.148982.

Lu, T., Xia, T., Qi, Y., Zhang, C., Chen, W., 2016. Effects of clay minerals on transport of graphene oxide in saturated porous media. Environ. Toxicol. Chem. 36, 655–660. https://doi.org/10.1002/etc.3605.

Maged, A., Kharbish, S., Ismael, I.S., Bhatnagar, A., 2020. Characterization of activated bentonite clay mineral and the mechanisms underlying its sorption for ciprofloxacin from aqueous solution. Environ. Sci. Pollut. Res Int 27, 32980–32997. https://doi.org/10.1007/s11356-020-09267-1.

Nie, X., Xing, X., Xie, R., Wang, J., Yang, S., Wan, Q., et al., 2023. Impact of iron/aluminum (hydr)oxide and clay minerals on heteroaggregation and transport of nanoplastics in aquatic environment. J. Hazard. Mater. 446 https://doi.org/10.1016/j.jhazmat.2022.130649.

Roberts, S.D., Powell, M.D., 2003. Reduced total hardness of fresh water enhances the efficacy of bathing as a treatment for amoebic gill disease in Atlantic salmon, Salmo salar L. J. Fish. Dis. 26, 591–599. https://doi.org/10.1046/j.1365-2761.2003.00495.x.

Shariati-Rad, M., Heidari, S., 2021. Partial least squares and silver nanoparticles in spectrophotometric prediction of total hardness of water. J. Chemom. 35 https://doi.org/10.1002/cem.3345.

Singh, N., Tiwari, E., Khandelwal, N., Darbha, G.K., 2019. Understanding the stability of nanoplastics in aqueous environments: effect of ionic strength, temperature, dissolved organic matter, clay, and heavy metals. Environ. Sci.: Nano 6, 2968–2976. https://doi.org/10.1039/c9en00557a.

Sun, H., Jiao, R., Wang, D., 2021. The difference of aggregation mechanism between microplastics and nanoplastics: role of brownian motion and structural layer force. Environ. Pollut. 268 https://doi.org/10.1016/j.envpol.2020.115942.

Torkzaban, S., Wan, J., Tokunaga, T.K., Bradford, S.A., 2012. Impacts of bridging complexation on the transport of surface-modified nanoparticles in saturated sand. J. Contam. Hydrol. 136-137, 86–95. https://doi.org/10.1016/j.jconhyd.2012.05.004.

Vu, T.T.T., Nguyen, N.T.T., Duong, L.H., Nguyen, A.D., Nguyen-Thanh, L., Dultz, S., et al., 2023. Coaggregation assisted by cationic polyelectrolyte and clay minerals as a strategy for the removal of polystyrene microplastic particles from aqueous solutions. Appl. Clay Sci. 233 https://doi.org/10.1016/j.clay.2023.106820.

Wang, X., Li, Y., Zhao, J., Xia, X., Shi, X., Duan, J., et al., 2020. UV-induced aggregation of polystyrene nanoplastics: effects of radicals, surface functional groups and electrolyte. Environ. Sci.: Nano 7, 3914–3926. https://doi.org/10.1039/d0en00518e.

Wu, Y., Cheng, Z., Wu, M., Hao, Y., Lu, G., Mo, C., et al., 2023. Quantification of two-site kinetic transport parameters of polystyrene nanoplastics in porous media. Chemosphere 338, 139506. https://doi.org/10.1016/j.chemosphere.2023.139506.

Xia, T., Lin, Y., Li, S., Yan, N., Xie, Y., He, M., et al., 2021. Co-transport of negatively charged nanoparticles in saturated porous media: Impacts of hydrophobicity and surface O-functional groups. J. Hazard. Mater. 409 https://doi.org/10.1016/j.jhazmat.2020.124477.

Xie, R.Y., Xing, X.H., Nie, X., Ma, X.S., Wan, Q., Chen, Q.S., et al., 2023. Deposition behaviors of carboxyl-modified polystyrene nanoplastics with goethite in aquatic environment: Effects of solution chemistry and organic macromolecules. Sci. Total Environ. 904, 166783 https://doi.org/10.1016/j.scitotenv.2023.166783.

Yang, X., An, C., Feng, Q., Boufadel, M., Ji, W., 2022. Aggregation of microplastics and clay particles in the nearshore environment: characteristics, influencing factors, and implications. Water Res. 224 https://doi.org/10.1016/j.watres.2022.119077.

Ye, X., Cheng, Z., Wu, M., Hao, Y., Lu, G., Hu, B.X., et al., 2022. Effects of clay minerals on the transport of polystyrene nanoplastic in groundwater. Water Res. 223, 118978 https://doi.org/10.1016/j.watres.2022.118978.

Yu, S.-j, Li, Q.-c, Shan, W.-y, Hao, Z.-n, Li, P., Liu, J.-f, 2021. Heteroaggregation of different surface-modified polystyrene nanoparticles with model natural colloids. Sci. Total Environ. 784 https://doi.org/10.1016/j.scitotenv.2021.147190.

Zeng, P., Nie, X., Qin, Z.H., Luo, S.X., Fu, Y.H., Yu, W.B., et al., 2023. Adsorption of gold nanoparticles on illite under high solid/liquid ratio and initial pH conditions. Clay Miner. 1–13. https://doi.org/10.1180/clm.2023.23.

Zhang, R., Chen, Y., Ouyang, X., Weng, L., Ma, J., Shafiqul Islam, M., et al., 2023. Resolving natural organic matter and nanoplastics in binary or ternary systems via UV–Vis analysis. J. Colloid Interface Sci. 632, 335–344. https://doi.org/10.1016/j.jcis.2022.11.050.

Zhang, Y., Luo, Y., Yu, X., Huang, D., Guo, X., Zhu, L., 2022. Aging significantly increases the interaction between polystyrene nanoplastic and minerals. Water Res. 219 https://doi.org/10.1016/j.watres.2022.118544.